processes

MDPI

Article

Modelling of Surface Roughness and Change in Out-of-Roundness of Tool during Electrical Discharge Machining with Cermet Tool Tip Using Machine Learning

Arminder Singh Walia [1], Vineet Srivastava [2,*] and Karun Verma [3]

[1] Department of Mechanical Engineering, Thapar Polytechnic College, Patiala 147004, India; arminderwalia@gmail.com
[2] Mechanical Engineering Department, Thapar Institute of Engineering and Technology, Patiala 147004, India
[3] Computer Science and Engineering Department, Thapar Institute of Engineering & Technology, Patiala 147004, India; karun.verma@thapar.edu
* Correspondence: vineet.srivastava@thapar.edu; Tel.: +91-98-8803-1148

Abstract: Surface roughness of the finished part and profile of the tool electrode are significant factors to assess the functionality of electrical discharge machining process. In this study, EDM was utilized for the machining of hardened EN31 steel. A sintered cermet tool tip with 75% copper–25% titanium carbide was fabricated and used as tool electrode. A data set of 262 such samples was developed with machining variables including discharge current (I_p), gap voltage (V_g), pulse on time (T_{on}), pulse off time (T_{off}) and flushing pressure (P). By correlating the machining variables, a machine learning-based regression model was developed for the prediction of surface roughness of the machined surface and change in out-of-roundness of tool during the EDM process. With the help of heat maps and a probability table, it was found that I_p, T_{on}, T_{off} and P had significant effect on SR, and I_p, T_{on} and T_{off} affected OOR. The machine learning-based regression equation predicted SR with average error of 1.6% and OOR with average error of 0.48%. It was found that machine learning-based regression equation had better accuracy as compared to a DOE-based regression equation.

Keywords: electrical discharge machining; surface roughness; change in out-of-roundness; discharge current; gap voltage; pulse on time; pulse off time; flushing pressure

Citation: Walia, A.S.; Srivastava, V.; Verma, K. Modelling of Surface Roughness and Change in Out-of-Roundness of Tool during Electrical Discharge Machining with Cermet Tool Tip Using Machine Learning. *Processes* **2022**, *10*, 252. https://doi.org/10.3390/pr10020252

Academic Editor: Antonino Recca

Received: 23 December 2021
Accepted: 24 January 2022
Published: 27 January 2022

1. Introduction

Electrical discharge machining (EDM) is an unconventional machining process primarily utilized in the manufacturing of dies that uses thermal erosion as the mechanism of material removal. In EDM, stock removal from specimen is performed using continuous discharges between tool and workpiece. It leads to creation of a plasma channel, and the temperature reaches up to 8000–20,000 °C, thereby removing the material from the electrodes by melting and evaporation [1–4]. In EDM, removal of material from a conducting workpiece takes place by a string of repeated electrical discharges within the workpiece and tool electrode in the existence of a dielectric liquid. A servo-controlled feed mechanism is used to move the electrode towards the workpiece until the gap is small enough to ionize the dielectric by the applied voltage. A discharge of very short duration is produced in a liquid dielectric gap, thus removing the material from the electrodes by heating, melting and evaporation. The next spark will be developed at the closest location between the tool tip and workpiece. This sparking process keeps changing its location all across the surface of the electrode tool tip, thereby creating an exact replica of the electrode profile on the workpiece [1]. Performance of the EDM process generally depends upon certain machine-dependent factors and user-specified factors. These factors include discharge current, breakdown voltage, gap voltage, pulse on/off duration, machining time, duty cycle, polarity, dielectric pressure, etc. Material removal rate (MRR), surface roughness (SR),

tool wear rate (TWR), surface integrity and dimensional accuracy of the finished product are certain parameters for evaluating the efficiency of the EDM process. These responses have been optimized using different mathematical models and statistical techniques such as dimensional analysis, artificial neural network (ANN), genetic algorithm (GA), response surface methodology (RSM), Taguchi method, fuzzy theory, finite element method (FEM) and regression analysis (RA), which ensures better results of the outcomes and efficiency.

Fenggou and Dayong [5] optimized ANN with GA and the node deletion algorithm to calculate process variables automatically. The use of genetic algorithms and back propagation (BP) algorithms enhanced the training speed of the model. Structure of the ANN was determined and optimized by node deletion algorithm. Rangajanardhaa and Rao [6] optimized the response of current and voltage on SR during EDM of Ti6Al4V, HE15, 15CDV6 and M-250. With the use of a package, a neural network model was generated. The use of GA to optimize the model further reduced the error to less than 2% from 5%. Chattopadhyay et al. [7] used the empirical model and predicted the SR of the surface machined with the EDM process. The range of maximum deviation for the prediction of response varied from 16.4% to −14.1%. The average prediction error for SR was found to be 0.05%. Torres et al. [8] performed the EDM of hard to machine alloy (Inconel 718) using copper electrode and proposed models for MRR, EWR and SR. The R^2 values obtained for MRR, SR and electrode wear rate (EWR) models were found to be 99.03%, 85.97% and 93.32%, respectively. The R^2 value indicates the adequacy of the developed model to link the relationship between EDM variables and responses. Raja et al. [9] applied firefly algorithm for the optimization of EDM process variables and to achieve the required surface roughness on hardened die steel workpiece in the least possible time. It was found that the influence of current on surface roughness and machining time was 45.53% and 37.53%, respectively, as compared to the influence of pulse duration on surface roughness and machining time being 1.37% and 1.04%, respectively. It was found that current influenced surface roughness and machining time more in comparison to pulse duration. Choudhuri et al. [10] optimized the process parameters for SR during the wire EDM of stainless steel. Grey relational technique was used to determine the grey coefficient of every experiment. Fuzzy evaluated the performance characteristics index in accordance with the grey relational coefficient. RSM and analysis of variance were utilized for modelling and analysis of SR to predict and determine the effect of machining variables.

Payal et al. [11] predicted MRR and SR during EDM of Inconel 825 with copper, copper–tungsten tools and graphite tools using ANN. ANN predicted the SR and MRR with an average percentage difference of 0.37 and 0.25, respectively. Nain et al. [12] evaluated the performance of wire EDM of aeronautics super alloy using fuzzy logic and backpropagation neural network. To analyse the scattering around the agreement line, two more lines in the range of ±5% error were plotted. For the evaluation of SR and waviness of the machined surface BP-ANN proved to be a better method. Thankachan et al. [13] used Taguchi and ANN to analyse and model MRR and SR during the wire EDM of aluminium-based metal matrix composite. Taguchi analysis revealed that the MRR increased with the percentage of tin and decreased with the rise in percentage of silicon carbide. Increase in SiC resulted in an increase in surface roughness, whereas the increase in tin resulted in a decrease in surface roughness. Sahu et al. [14] investigated the influence of process variables on overcut and SR during the EDM of Al–SiC composite. Copper was used as a tool electrode. RSM and MOPSO were used for the mathematical modelling of responses and multiresponse optimization, respectively. Decrease in SR was recorded with the rising flushing pressure and pulse off time. To decrease the overcut, lower pulse durations and higher voltage settings were suggested. Rajneesh et al. [15] reported the EDM of AISI 202 stainless steel with copper alloy tool. RSM was utilized to optimize MRR, EWR and SR. Current and pulse on/off were selected as process variables. Regression equations were formed, and interactive effects of process variables were analysed. R^2 was used to check the goodness of fit. The R^2 was calculated and found to be 95.09%, 95.05% and 96.68% for EWR, MRR and SR, respectively. Singh and Singh [16] developed a semiempirical

model for the prediction of SR during the EDM process. The model was successful in predicting the response with lesser than 5% error. Ulas et al. [17] predicted SR using extreme learning machine and support vector regression-based models. Weighted extreme learning machine model was found as the best model with R^2 value of 0.9720. Bharti [18] applied two-step optimization processes to find out the optimal parameters for EDM. Neural network-based multi-objective optimization technique was employed to generate the total possible combinations of input parameters. By applying the concept of dominance, 24 nondominated combinations of input parameters were obtained. TOPSIS was used to award rank to each nondominated solution.

Srivastava and Pandey [19] studied the process performance of sintered copper (Cu)–titanium carbide (TiC) electrode tip in ultrasonic-assisted cryogenically cooled electrical discharge machining (UACEDM). The performance parameters evaluated were electrode wear ratio (EWR), material removal rate (MRR), surface roughness (SR), out-of-roundness and surface integrity. The process parameters considered in this study are discharge current, pulse on time, duty cycle and gap voltage. Cermet was fabricated, having a copper content of 75% and titanium carbide content of 25%, by mixing, pressing and sintering. It was observed that EWR and out-of-roundness decreased when the cermet electrode tip was used as compared to a conventional tool tip. It was also observed that MRR and SR increased when the cermet tool tip was used. The surface cracks' density and crack width on a workpiece machined by a cermet tool tip have been found to be lesser as compared to the specimen machined by a conventional tool tip. Srivastava and Pandey [20] studied the shape of the electrode and established the application of liquid nitrogen in reducing distortion of the electrode during electrical discharge machining of M2-grade high-speed steel using copper electrodes. A study of roundness was performed on the electrode to observe the shape of the electrode for both conventional EDM and EDM with a cryogenically cooled electrode. A scanning electron microscope (SEM) was used to study the shape of the electrode tip. The effect of various parameters such as discharge current and pulse on time were studied to understand the behaviour of distortion of the electrode. It was concluded that the shape retention was better in the case of a liquid nitrogen-cooled electrode. Srivastava and Pandey [21] studied the cooling effect on copper electrodes while electrical discharge machining (EDM) an M2-grade high-speed steel workpiece. To evaluate the machinability, electrode wear ratio (EWR) and surface roughness (SR) were the two responses observed. Discharge current, pulse on time, duty cycle and gap voltage were the controllable process parameters. It was found that EWR reduced up to 20% by cryogenic cooling the electrode. With electrode cooling, SR was also found to have been reduced after machining. The effect of process parameters on EWR and SR were also analysed. The shape of the electrode was also measured, and it was found that the shape retention was better in cryogenic-assisted EDM as compared to conventional EDM.

It was found from the investigation of literature that a lot of research work is being done for the prediction of responses, whereas there is still a lack of literature available that highlights the use of change in out-of-roundness of the cermet tool tip and for predicting surface roughness of the machined workpiece, especially during the EDM of the hard workpiece. Surface roughness is an important criterion while evaluating the outcome of EDM, as it has a significant influence on the mating parts. The change in the shape of the tool during machining is very significant, as the final shape of the machined cavity is dependent on the shape of the tool during EDM. There are very few studies that analysed the change in the shape of the tool [20–22]. Therefore, the present study is focused on investigating the surface roughness of the machined cavity and the change in the tool's shape by observing the changes in out-of-roundness of the tool with changing process parameters. A novel approach to use machine learning techniques for the prediction of the mentioned responses has been attempted through this work.

2. Materials and Methods

To analyse the surface roughness and out-of-roundness of the tool, experiments were performed on a die sinking EDM machine. The cermet tool tip was utilized for machining of a hardened EN31 workpiece. The entire process is detailed below.

2.1. Workpiece and Tool Material

In this work, hardened EN31 steel was selected as the workpiece material due to its high hardness and abrasion resistance, which makes it difficult to machine. For experimentation, the samples of EN31 steel with a size of 15 mm × 15 mm × 6 mm were used. The hardness of EN31 steel was found to be 20 HRC, which was further enhanced to 56 HRC after heat treatment. The objective of heat treatment was to make the workpiece more difficult to machine under normal machining conditions. The parameters used for the heat treatment of workpiece are presented in Table 1. The chemical composition of EN31 steel after heat treatment was determined by evaluating the average of 20 workpiece samples assessed using energy dispersive X-ray spectroscopy (EDAX) and was found to be C-2.09%, Si-0.32%, Mn-0.62%, Cr-1.14%, S-0.035%, P-0.026%, Fe-95.76%.

Table 1. Heat treatment parameters [22].

Parameter	Hardening	Tempering
Hardening temperature	850 °C	-
Tempering temperature	-	260 °C
Soaking time	20 min	1 h
Heating rate	600 °C/h	600 °C/h

Copper (Cu) is widely accepted tool electrode material in the EDM process. However, in machining hard materials, higher tool wear of copper tools raises the need of another material that can be used more efficiently. High melting temperature, high hardness, excellent thermal shock and wear resistance make titanium carbide (TiC) an ideal option for reinforcement material for the cermet tool tip [23]. From the literature survey [24–26] and pilot experiments conducted, the composition of copper and titanium carbide was fixed at 75 and 25%, respectively. The purity of copper powder was 99.9%, and that of TiC was 99.8%. The average grain size for both the powders was 44 µm. The procedure for the fabrication of cermet tool tip electrode is given in Figure 1. The electrical resistivity of the developed tool tip was 5.056 µΩcm, thermal conductivity was 141.96 W/m·K, microhardness was 126.78 HV and relative density was 0.89. The sintered polished pellets of 10 mm diameter were brazed to the copper rods (as shown in Figure 2) and were used as the cermet tool tip electrode.

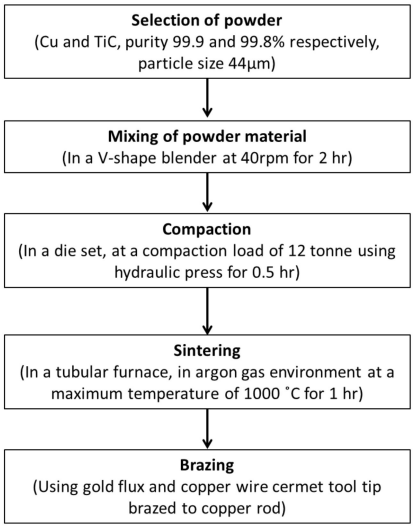

Figure 1. Procedure of fabrication of the cermet tool tip electrode.

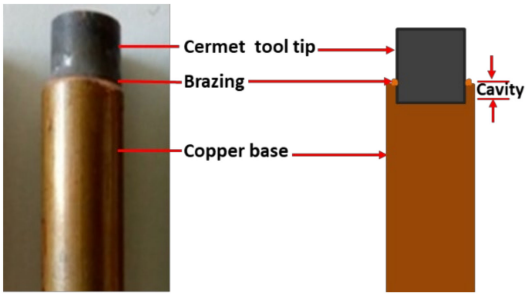

(**a**)

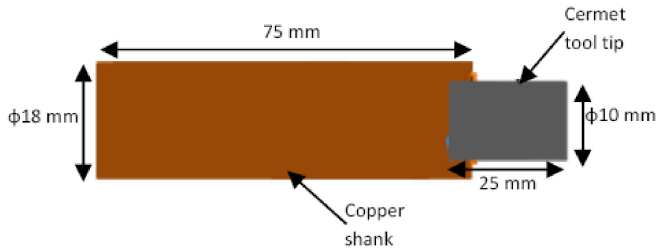

(**b**)

Figure 2. (**a**) Cermet tool tip electrode developed (**b**) Dimensional details of the electrode [21].

2.2. Selection of Process Parameters and Data Generation

EN31 tool steel workpieces were machined using die sinking EDM (Reliable, 55,300). The commercially available EDM oil (flashpoint: 90 °C; SG: 0.77) was used as the dielectric medium for experimentations. Based on the capability of machine and pilot experiments, five variables, viz., discharge current, gap voltage, pulse on time, pulse off time and flushing pressure, were selected. The discharge current below 3 A results in much less MRR, and the discharge current above 11 A results in higher surface roughness. Pulse on time (T_{on}) and pulse off time (T_{off}) were kept in the range based on the available literature and are generally used in the EDM process for steel. The range of gap voltage and flushing pressure was chosen in accordance with the range available on the machine selected for the experimentation. The experimental machining parameters used in the present work are shown in Table 2. By varying the variables in the selected range, experiments were performed. The duration of machining was fixed at 30 min for each experiment.

Table 2. Machining variable.

Experimental Parameter	Ranges/Values for Experimentation
Discharge current, I_p	3–11 A, step size: 1 A
Gap voltage, V_g	40–80 V, step size: 5 V
Pulse on time, T_{on}	100–500 µs, step size: 50 µs
Pulse off time, T_{off}	10–50 µs, step size: 5 µs
Flushing pressure, P	12–20 kgf/cm^2, step size: 1 kgf/cm^2

Surface roughness has considerable influence on properties such as fatigue, strength and resistance to wear. It is one of the most significant measures in finishing operation. It is, therefore, important to achieve a good surface finish. A surface roughness tester (Surftest SJ400, Mitutoyo South Asia Pvt. Ltd., New Delhi, Delhi, India) was used to measure the surface roughness. As per industry standards [27], centre line average value of surface roughness (R_a) was used in the present study. The traverse length of 4 mm with a cut-off evaluation length of 0.8 mm was used. Each sample was measured 5 times, and their average was taken as the response. The surface roughness profile of one the machined cavity is shown in Figure 3.

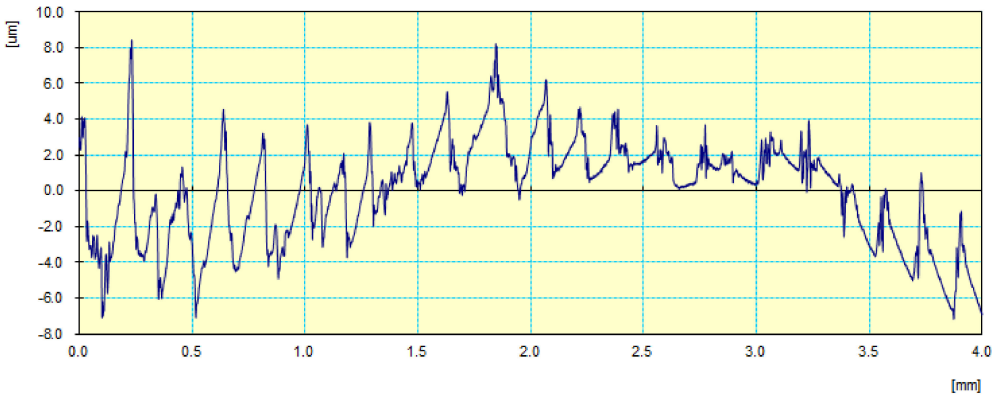

Figure 3. Surface roughness profile (I_p, V_g, T_{on}, T_{off}, P) = (5, 70, 200, 20, 19); units as per Table 2.

In the EDM process, the edges of the tool sometimes get changed from sharp to round, and the shape of the edges of the tool also become affected due to wear. The overall effect is the change in the roundness of the tool, which, in turn, affects the profile of the machined cavity. Coordinate measuring machine (CMM, Accurate, model Spectra 564) and Accusoft plus software were used for analysing the data to evaluate the change in OOR. Out-of-roundness, shown as Equation (1), is measured as the radial difference between the two concentric circles enclosing all the measured data points [28].

$$OOR = r_{max} - r_{min} \quad (1)$$

The schematic of tool profile is shown in Figure 4a. The measurement of out-of-roundness using CMM is presented in Figure 4b.

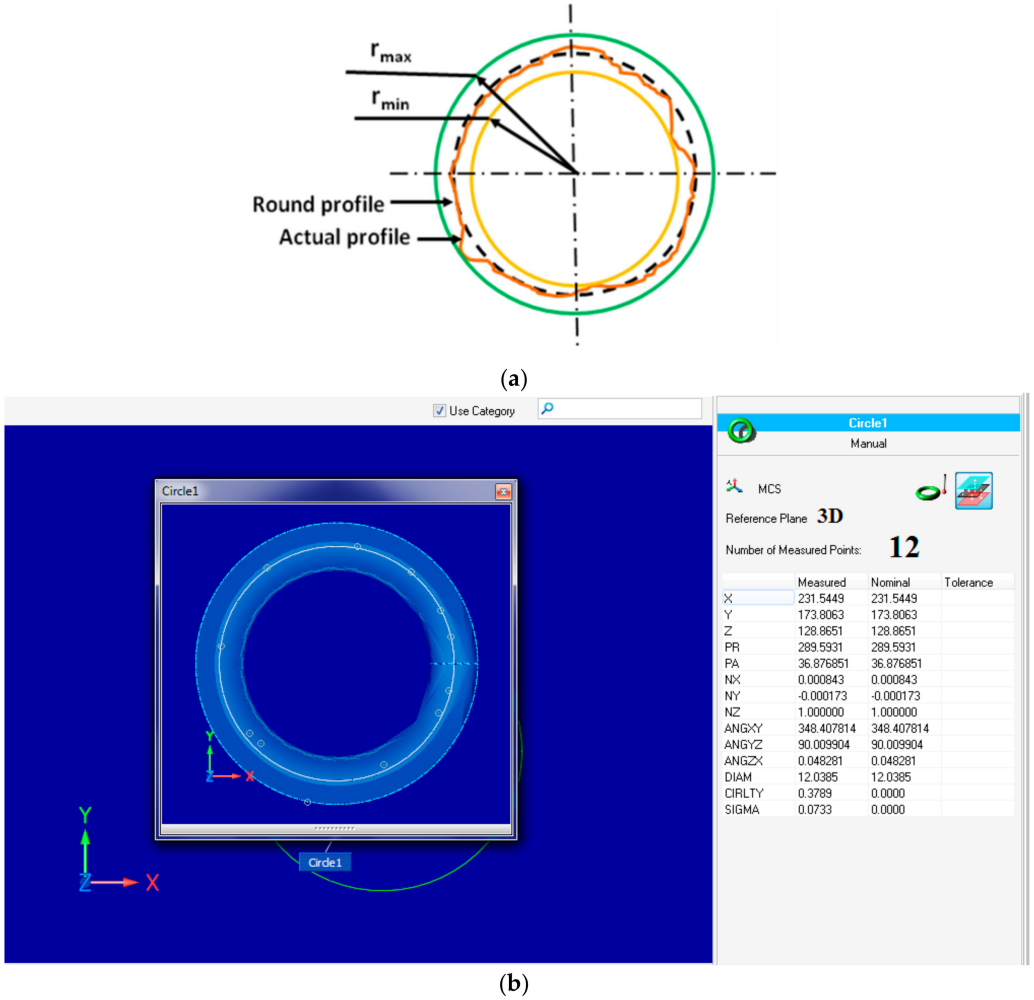

Figure 4. (**a**) Schematic of tool profile [21]. (**b**) Measurement of OOR using CMM.

To evaluate the change in the shape of the tool, measurement of roundness was twice, once before and another after machining on both a copper as well as a cermet tool tip. This measurement was performed at 12 points across the circumference of the tip for each sample using CMM, and the value of roundness was recorded.

In this work, initially, the cermet tool tip was fabricated and brazed to the copper shank. Meanwhile, the EDM process parameters were defined. Then, using single variable experiments, the experimental process settings were finalized. During EDM, commercially available EDM oil was used as the dielectric, and machining time was fixed at 30 min based on preliminary experimentations. The measured results for the surface roughness (SR) of the machined cavity and change in out-of-roundness (OOR) of the tool during the EDM process are shown in Table A1 in Appendix A. By using the 262 sample measurements generated from the experiments, Python software was used to develop a quadratic regression curve. The program was run on 215 sample measurements as the training set. The other 47 samples were used for validation of the regression curve by comparing the predicted values with the experimentally measured output. The regression curve returned the coefficients of 20 expressions for 5 different dependant parameters along with a constant.

3. Results and Discussion

3.1. Modelling of Surface Roughness

A machine learning-based regression model was trained for the prediction of SR by correlating the input variables. In order to train the machine learning model, we derived quadratic features out of the five machining variables, which generated a 20-tuple input

vector for training. The 20-tuple vector consisted of five machining variables, their square terms and the interaction of different machining variables with each other. The coefficients obtained for input variables are presented in Table 3. The value of intercept (constant) was found to be 4.5245. The developed regression equation for SR is given below in Equation (2).

$$\begin{aligned} SR = 4.5245 \quad & -(0.2506 \times I_p) + (0.0112 \times V_g) - (0.0057 \times T_{on}) \\ & +(0.0266 \times T_{off}) + (0.1859 \times P) + \left(0.0082 \times I_p^2\right) \\ & -\left(0.0002 \times V_g^2\right) - \left(1.948 \times 10^{-5} \times T_{on}^2\right) - \left(0.0002 \times T_{off}^2\right) \\ & -\left(0.0088 \times P^2\right) + (6.45 \times 10^{-5} \times I_p \times V_g) \\ & +(0.008 \times I_p \times T_{on}) + (0.0001 \times I_p \times T_{off}) \\ & +(0.0062 \times I_p \times P) + (5.45 \times 10^{-5} \times V_g \times T_{on}) \\ & -(2.109 \times 10^{-5} \times V_g \times T_{off}) - (0.0001 \times V_g \times P) \\ & -(4.583 \times 10^{-7} \times T_{on} \times T_{off}) - (1.087 \times 10^{-5} \times T_{on} \times P) \\ & +(0.0001 \times T_{off} \times P) \end{aligned} \tag{2}$$

Table 3. Coefficients of variables for SR model.

Variable	Coefficient	Variable	Coefficient
I_p	−0.2506	$V_g \times V_g$	−0.0002
V_g	0.0112	$V_g \times T_{on}$	5.45×10^{-5}
T_{on}	−0.0057	$V_g \times T_{off}$	-2.109×10^{-5}
T_{off}	0.0266	$V_g \times P$	−0.0001
P	0.1859	$T_{on} \times T_{on}$	-1.948×10^{-8}
$I_p \times I_p$	0.0082	$T_{on} \times T_{off}$	-4.583×10^{-7}
$I_p \times V_g$	6.45×10^{-5}	$T_{on} \times P$	-1.087×10^{-5}
$I_p \times T_{on}$	0.0008	$T_{off} \times T_{off}$	−0.0002
$I_p \times T_{off}$	0.0001	$T_{off} \times P$	0.0001
$I_p \times P$	0.0062	$P \times P$	−0.0088

In order to determine the significance of various input vectors with respect to SR, a heat map was developed (Figure 5). The map shows the various interactions of the input vectors with respect to SR. The table highlighting the coefficients and probability is given in Table 4. In Table 4, Coef is the coefficient of variable in regression equation, Std_err is the standard error, T is the value of coefficient divided by Std_err and P is the probability value describing the T distribution. On evaluating the heat map and the probability table, it was found that I_p, V_g, T_{on}, T_{off}, P, $I_p{}^2$, $V_g{}^2$, $T_{on}{}^2$, $T_{off}{}^2$, $I_p \times V_g$, $I_p \times T_{off}$, $V_g \times T_{on}$, $T_{on} \times P$, $T_{off} \times P$ were significant and influence the SR.

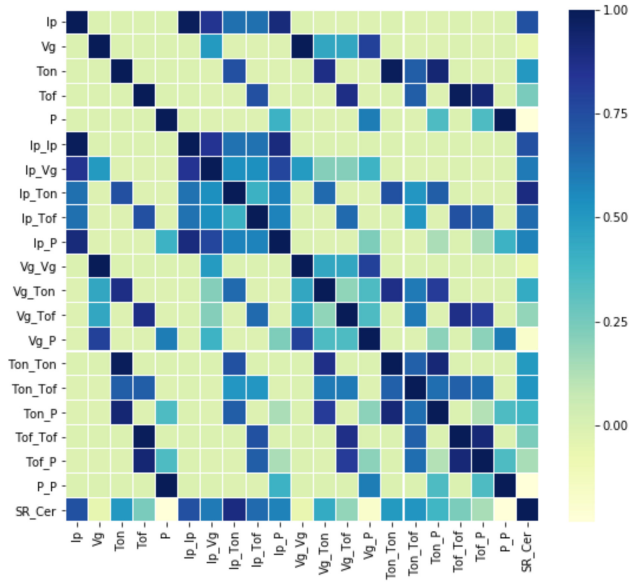

Figure 5. Heat map for SR.

Table 4. Coefficients and probability for SR model.

	Coef	Std_err	T	P > |t|
I_p	−0.2506	0.013	−19.740	0.000
V_g	0.0112	0.003	3.592	0.000
T_{on}	−0.0057	0.000	−23.296	0.000
T_{off}	0.0266	0.002	10.263	0.000
P	0.1859	0.018	10.106	0.000
$I_p \times I_p$	0.0082	0.001	16.150	0.007
$I_p \times V_g$	-6.45×10^{-5}	-9.09×10^{-5}	0.710	0.479
$I_p \times T_{on}$	0.0008	9.09×10^{-6}	84.332	0.000
$I_p \times T_{off}$	0.0001	9.09×10^{-5}	1.213	0.226
$I_p \times P$	0.0062	0.000	13.603	0.000
$V_g \times V_g$	−0.0002	2.04×10^{-5}	−11.587	0.000
$V_g \times T_{on}$	5.405×10^{-5}	1.82×10^{-6}	29.723	0.000
$V_g \times T_{off}$	-2.109×10^{-6}	1.82×10^{-5}	−0.116	0.908
$V_g \times P$	−0.0001	9.09×10^{-5}	−1.578	0.116
$T_{on} \times T_{on}$	-1.948×10^{-8}	2.03×10^{-7}	−0.096	0.924
$T_{on} \times T_{off}$	4.583×10^{-7}	1.82×10^{-6}	−0.252	0.801
$T_{on} \times P$	-1.087×10^{-5}	9.09×10^{-6}	−1.196	0.233
$T_{off} \times T_{off}$	−0.0002	2.03×10^{-5}	−12.157	0.000
$T_{off} \times P$	0.0001	9.09×10^{-5}	1.337	0.182
$P \times P$	−0.0088	0.001	−17.344	−0.010

The individual and interaction effects of all the parameters of the predictive model are shown in Figure 6. The I_p is the individual with the maximum contribution of 13.06%. The T_{on}, T_{off} and P have a share of 7.47%, 3.97% and 3.91%, respectively. Significant interaction effects of I_p, T_{on}, T_{off} and P can be observed in Figure 6. The V_g had a contribution of

1.39%. The interaction effect of V_g had maximum significance of 1.83% only. Thus, it can be concluded that the I_p, T_{on}, T_{off} and P are the main parameters influencing the SR.

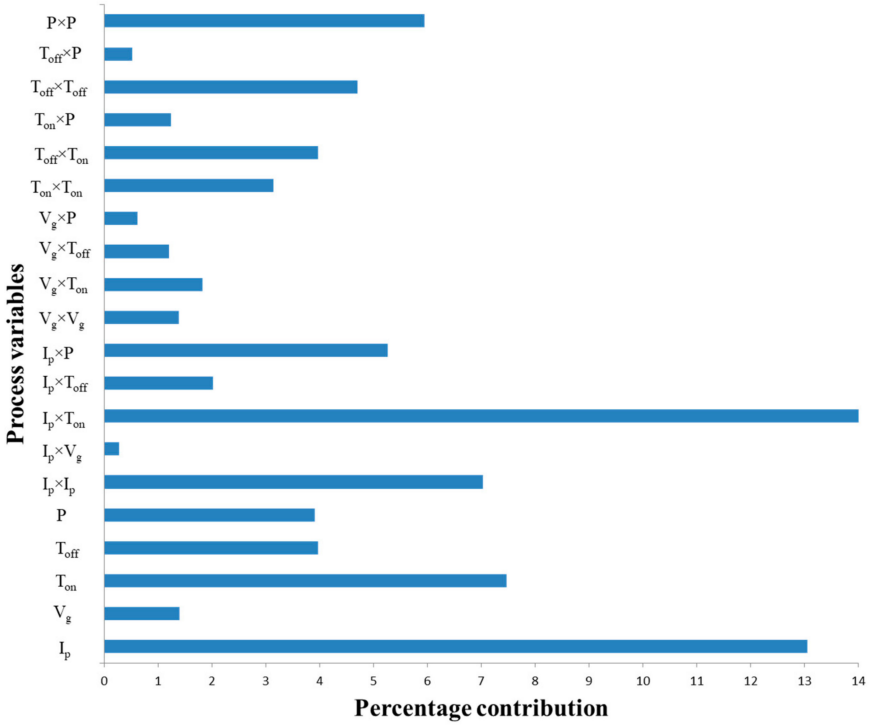

Figure 6. Percentage influence of process variables and interactions on SR.

3.2. Main Effect Plots for Machine Learning Model for Surface Roughness

It is very difficult to differentiate whether the whole surface is recast or if there is a portion of a recast layer. The best way is utilize energy dispersive X-ray spectroscopy (EDAX). In the EDM process, there is a distinct formation of a layer at the top of the machined surface. This layer is formed from the accumulation of carbon, which is generated from the cracking of dielectric and the resolidification of the molten material left in the machined cavity after flushing. Thus, evaluating the developed surface formed in Figures 8, 10, 12 and 14 using EDAX, it is observed that there is a very significant increase in carbon content in addition to all the elements of the workpiece. The EDAX of the machined surface, especially the zone marked as the recast layer, gave the following composition: C-16-20%, Cr-0.65-0.95%, Si-0.18-0.62%, Mn-0.2-0.62%, S-0.12-0.28%, P-0.09-0.22%, Cu-1.66-2.94%, O-2.6-5.15%, Ti-<1%, Fe-69.53-75.85%. On the machined surface, presence of Cu and Ti is due to some tool electrode deformation because of high temperatures in the machining zone. The presence of O is due to some oxidation and decomposition in the removal of the material from the workpiece surface. The carbon enrichment can be explained by the deposition of carbon estranged from the dielectric consumed as a result of cracking of dielectric [29]. However, the presence of other elements can be there only if they were extracted out of the workpiece. Therefore, those areas were marked as recast layers in the figures.

The variation in SR during EDM with change in I_p is shown in Figure 7. It can be perceived that the plots obtained by using the DOE model [30] and machine learning model reveal similar developments. The SR of the machined cavity increased with a higher I_p. This can be due to the fact that increases in I_p result in an increase of the discharge energy density and impulsive forces [31]. This, in fact, causes the formation of large craters, which upsurges SR. Lesser surface irregularities are produced at low I_p during EDM. Furthermore, insignificant molten material is obtained between the work electrode and the tool electrode. All these contribute to attain a lower SR at a low I_p. Figure 8a shows an increase in SR due to the accumulation of more globules around the machining zone. Small-sized craters are

formed while performing EDM at low I_p, and less amount of eroded material is present in the gap between electrodes. A cavity with lesser surface irregularities is obtained at a lower I_p due to these reasons. Apart from this, sometimes the higher quantity of material removed during EDM at higher I_p is not efficiently removed by the dielectric fluid during flushing and produces a cavity with higher SR. The same can be observed from Figure 8b.

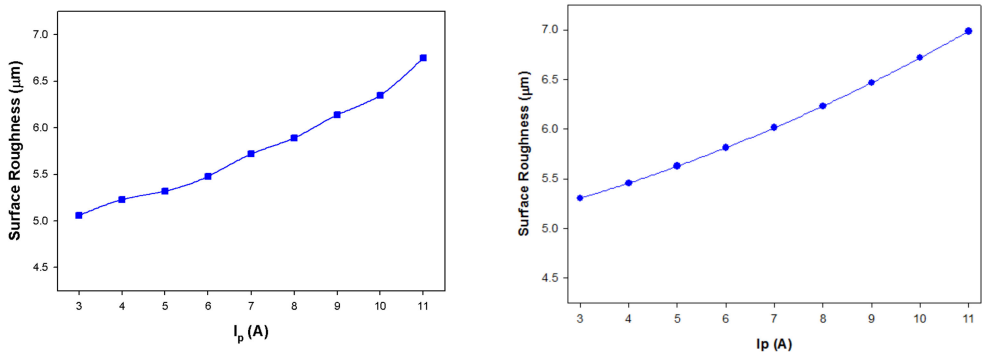

(**a**) (**b**)

Figure 7. Main effect plots for SR with I_p using (**a**) DOE model; (**b**) machine learning model.

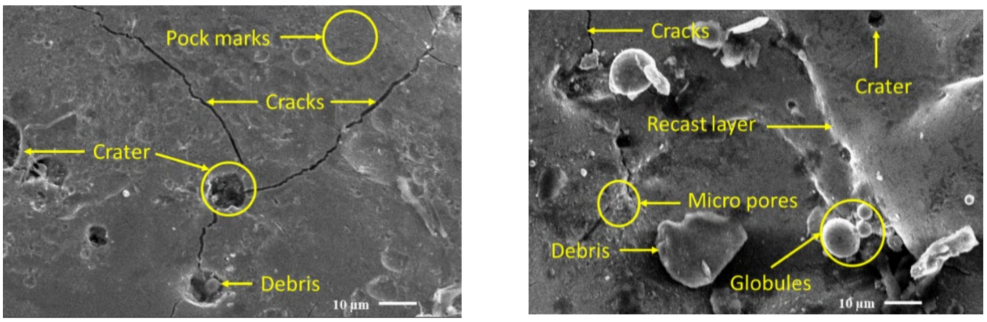

(**a**) (**b**)

Figure 8. Variation of surface morphology with I_p (I_p, V_g, T_{on}, T_{off}, P) (**a**) (6, 60, 300, 30, 16); (**b**) (10, 60, 300, 30, 16) units per Table 2.

The effect of Ton over SR is shown in Figure 9. As the Ton increased, the SR increased. The plasma channel increased at a larger pulse duration, which, in turn, decreased the energy density and impulsive force. The melted debris cannot be removed completely due to a reduction in impulsive force and forms a recast layer to degrade the surface roughness. At a shorter Ton, the material removed during a pulse is less. This small amount of material can efficiently be handled by flushing, resulting in the lower SR.

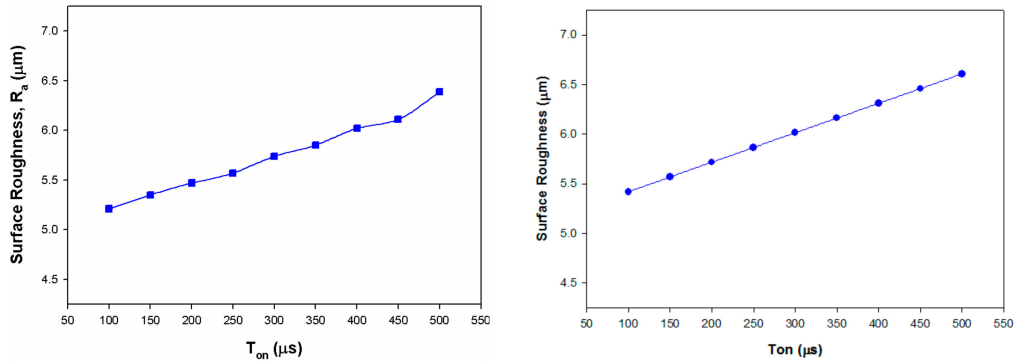

(**a**) (**b**)

Figure 9. Main effect plots for SR with T_{on} using (**a**) DOE model; (**b**) machine learning model.

The SEM of the cavity machined at a small value of Toff can be seen in Figure 10a. At smaller pulse durations, significantly lesser material is removed from the site more conveniently, resulting in lesser SR. Conversely, due to a reduction in forces at larger T_{on}, molten material is not evacuated completely from the cavity and piles up there, as shown in Figure 10b. This creates an observable globule-like recast layer and increases the SR. Moreover, micropores are formed due to the increase in Ton, which further add up to the SR. Lager pulse durations also cause the appearance of large-sized craters.

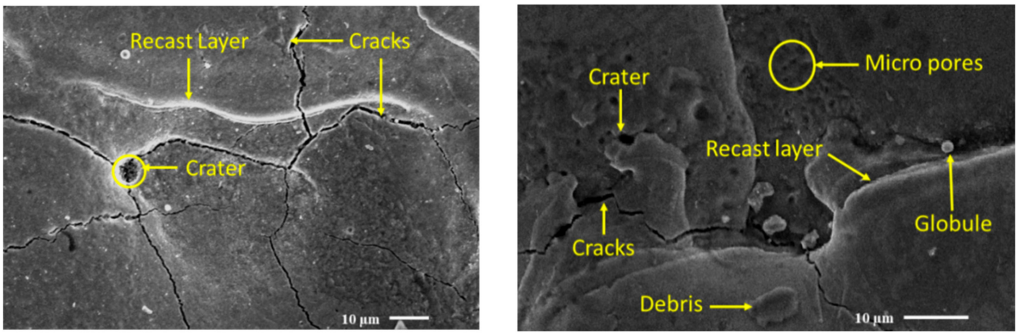

(**a**) (**b**)

Figure 10. Variation of surface morphology with Ton (I_p, V_g, T_{on}, T_{off}, P) (**a**) (7, 60, 250, 30, 16); (**b**) (7, 60, 450, 30, 16); units as per Table 2.

The relation of Toff with SR is shown in Figure 11. SR tends to increase with the increase in T_{off}. There is a considerable temperature drop on the tool and workpiece surface when the T_{off} is large. Consequently, to re-establish the plasma channel, more energy is needed, resulting in some portion of the energy consumed for this recreation. Thus, the net energy in the system decreased, causing inefficient disposal of debris and increasing the SR.

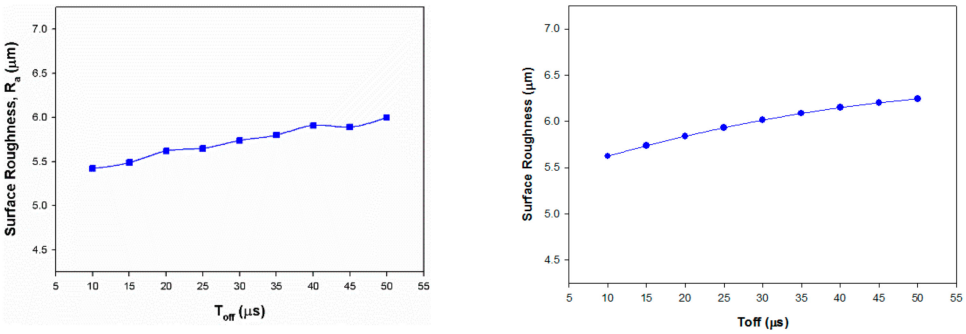

(**a**) (**b**)

Figure 11. Main effect plots for SR with T_{off} using (**a**) DOE model; (**b**) machine learning model.

The SEM images in the Figure 12 show the effect of the T_{off} on the SR of the machined cavity. The flushing process is affected during shorter pulse intervals due to the start of fresh machining even before the debris has been cleared. It results in the re-solidification of debris and the formation of a recast layer on the surface machined. It plugs up the microcracks and micropores, thereby assisting in reducing the SR. However, at the larger pulse off time (Figure 12b), the decrease in the available energy increases the surface irregularities. Larger sized pores are formed at higher T_{off}, resulting in increased SR.

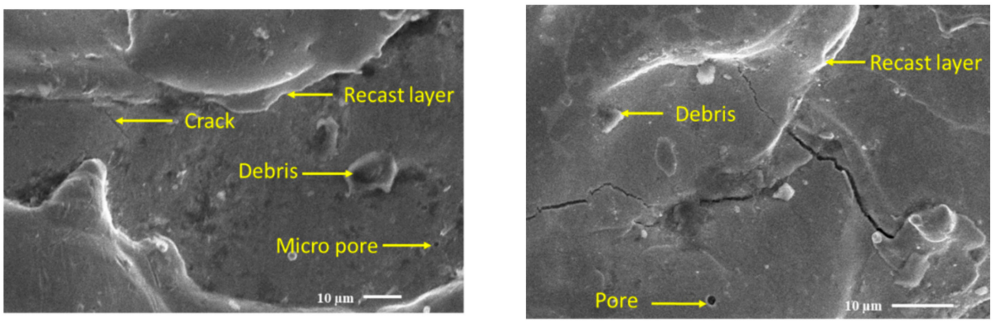

(**a**) (**b**)

Figure 12. Variation of surface morphology with T_{off} (I_p, V_g, T_{on}, T_{off}, P) (**a**) (7, 60, 300, 25, 16); (**b**) (7, 60, 300, 45, 16); units as per Table 2.

The impact of P on SR is shown in Figure 13. A decrease in SR can be seen with an increase in P. Due to smaller actuation of the dielectric, the wreckage produced during machining is not effectively evacuated at lower P. However, as the P is increased, debris is successfully removed, resulting in lower SR. This also results in ejection of removed material during machining due to big hydraulic force wielded on the machined cavity. From the Figure 14, it can be seen that the surface irregularities decreased with the increasing P. When the P is low, the debris produced is not taken away from the site of machining, as it is shown in Figure 14a. However, as the P increases, the efficient removal of debris from the cavity (Figure 14b) also reduces the chances of arcing during EDM and decreases the SR.

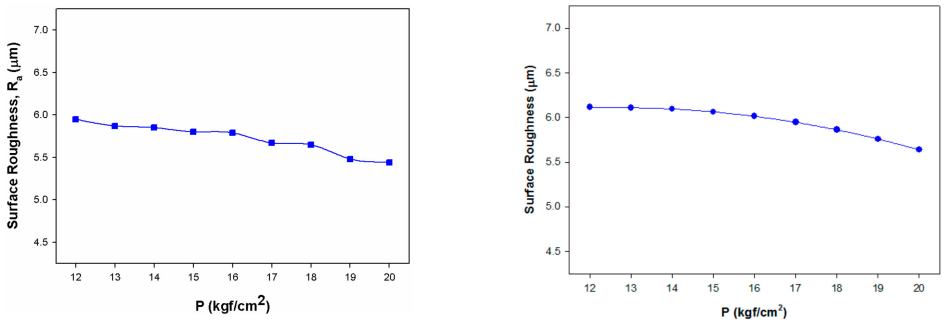

(**a**) (**b**)

Figure 13. Main effect plots for SR with P using (**a**) DOE model; (**b**) machine learning model.

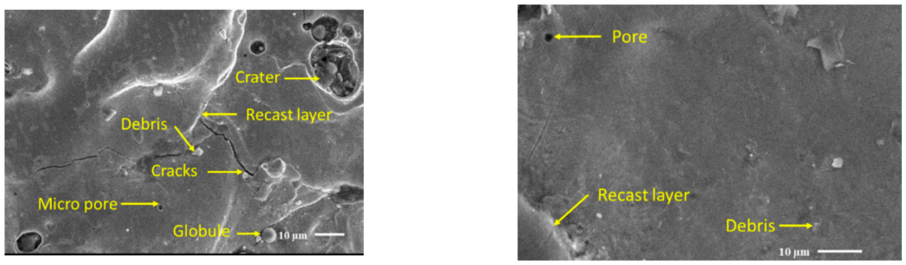

(**a**) (**b**)

Figure 14. Variation of surface morphology with P (I_p, V_g, T_{on}, T_{off}, P) (**a**) (7, 60, 300, 30, 13); (**b**) (7, 60, 300, 30, 19); units as per Table 2.

3.3. Modelling of Change in Out-of-Roundness

A machine learning-based regression model was developed for change in OOR by correlating the input parameters. In order to train the machine learning model, we derived quadratic features out of the five machining variables, which will generate a 20-tuple input vector for training. The 20-tuple vector consists of five machining variables, their square

terms and the interaction of different machining variables with each other. The coefficients obtained for input variables are presented in Table 5. The value of intercept (constant) was found to be −5.92. The developed regression equation for change in ORR is given below as Equation (3).

$$\begin{aligned}\text{Change in OOR} = \; & -5.92 + \left(2.94 \times I_p - \left(6.09 \times 10^{-2} \times V_g\right) + \left(0.123 \times T_{on}\right)\right. \\ & -\left(0.405 \times T_{off}\right) - \left(0.707 \times P\right) + \left(0.187 \times I_p^2\right) \\ & +\left(1.14 \times 10^{-4} \times V_g^2\right) - \left(6.8 \times 10^{-7} \times T_{on}^2\right) \\ & +\left(0.00287 \times T_{off}^2\right) + \left(2.36 \times 10^{-3} \times P^2\right) - \left(0.0205 \times I_p \times V_g\right) \\ & -\left(0.00402 \times I_p \times T_{on}\right) - \left(0.0207 \times I_p \times T_{off}\right) \\ & +\left(0.00692 \times I_p \times P\right) - \left(4.99 \times 10^{-4} \times V_g \times T_{on}\right) \\ & -\left(4.99 \times 10^{-4} \times V_g \times T_{off}\right) + \left(0.032 \times V_g \times P\right) \\ & +\left(0.001 \times T_{on} \times T_{off}\right) - \left(0.005 \times T_{on} \times P\right) \\ & +\left(4.8 \times 10^{-4} \times T_{off} \times P\right)\end{aligned} \tag{3}$$

Table 5. Coefficients of variables for change in OOR model.

Variable	Coefficient	Variable	Coefficient
I_p	2.94	$V_g \times V_g$	1.14×10^{-4}
V_g	-6.09×10^{-2}	$V_g \times T_{on}$	-4.99×10^{-4}
T_{on}	0.123	$V_g \times T_{off}$	-4.99×10^{-4}
T_{off}	−0.405	$V_g \times P$	0.032
P	−0.707	$T_{on} \times T_{on}$	-6.80×10^{-7}
$I_p \times I_p$	0.187	$T_{on} \times T_{off}$	0.001
$I_p \times V_g$	−0.0205	$T_{on} \times P$	−0.0050
$I_p \times T_{on}$	−0.00402	$T_{off} \times T_{off}$	0.00287
$I_p \times T_{off}$	−0.0207	$T_{off} \times P$	4.80×10^{-4}
$I_p \times P$	0.00692	$P \times P$	2.36×10^{-3}

In order to determine the significance of various input vectors with respect to change in OOR, a heat map was developed. The heat map is presented in Figure 15. The heat map shows the various interactions of the input vectors with respect to change in OOR. The table highlighting the coefficients and probability is given in Table 6. In Table 6, Coef is the coefficient of variable in regression equation, Std_err is the standard error, T is the value of coefficient divided by Std_err and P is the probability value describing the T distribution. On evaluating the heat map and the probability, it was found that I_p, V_g, T_{on}, T_{off}, P, T_{on}^2, T_{off}^2, V_g^2, P^2, $I_p \times V_g$, $I_p \times T_{on}$, $I_p \times T_{off}$, $V_g \times T_{on}$, $V_g \times P$, $T_{on} \times T_{off}$, $T_{on} \times P$, $T_{off} \times P$ were significant and influence the OOR.

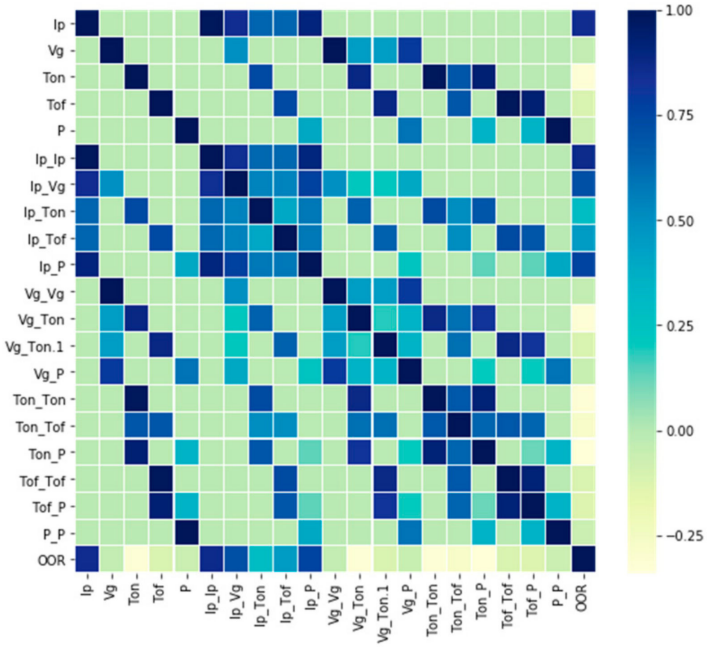

Figure 15. Heat map for change in OOR.

Table 6. Coefficients and probability for change in OOR.

	Coef	Std_err	T	P > |t|
I_p	2.7950	0.123	22.696	0.000
V_g	−0.1129	0.025	−4.485	0.000
T_{on}	0.1199	0.002	49.330	0.000
T_{off}	−0.4267	0.022	−19.528	0.000
P	−1.1015	0.106	−10.384	0.000
$I_p \times I_p$	0.1927	0.006	35.010	0.379
$I_p \times V_g$	−0.0246	0.001	−25.531	0.000
$I_p \times T_{on}$	−0.0040	9.75×10^{-5}	−41.049	0.000
$I_p \times T_{off}$	−0.0205	0.001	−21.045	0.000
$I_p \times P$	0.0093	0.005	1.95200	0.052
$V_g \times V_g$	0.0004	0.000	2.006	0.046
$V_g \times T_{on}$	−0.0005	9.68×10^{-5}	−51.250	0.000
$V_g \times T_{on}$	−0.0005	9.68×10^{-5}	−51.250	0.000
$V_g \times P$	0.0327	0.001	36.012	0.000
$T_{on} \times T_{on}$	1.1319×10^{-6}	2.22×10^{-6}	0.595	0.553
$T_{on} \times T_{off}$	0.0010	1.95×10^{-5}	51.431	0.000
$T_{on} \times P$	−0.0050	9.59×10^{-5}	−51.648	0.000
$T_{off} \times T_{off}$	0.0031	0.000	13.827	0.000
$T_{off} \times P$	0.0009	0.001	0.933	0.352
$P \times P$	0.0118	0.004	2.886	0.004

Figure 16 depicts the individual and interaction effects of all the parameters of the predictive model. The I_p is the individual with the maximum contribution of 13.15%. The T_{on} and T_{off} have a share of 9.30%, and 5.39%, respectively. A significant interaction effect

of I_p, T_{on} and T_{off} can also be observed from the figure. The V_g had a contribution of 0.94%, and P had a contribution of 1.09%. The interaction effects of V_g and P have a maximum significance of 3.54% only. After analysis, it can be concluded that I_p, T_{on} and T_{off} are the main parameters influencing the OOR.

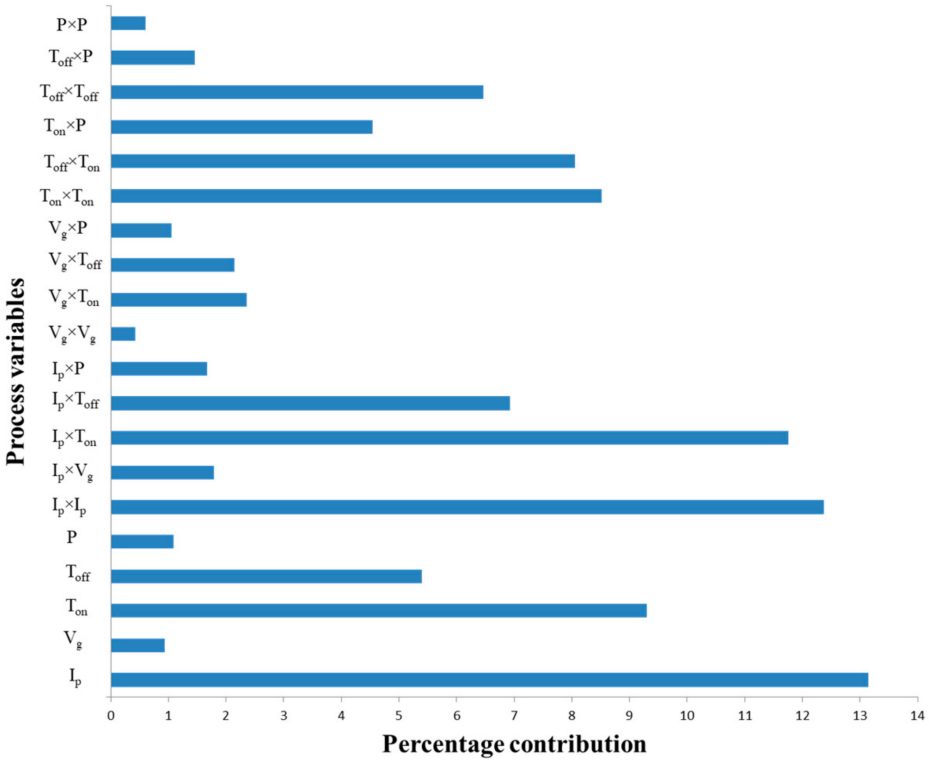

Figure 16. Influence of process variables and interactions on OOR (in %).

3.4. Main Effect Plots for Machine Learning Model for Change in Out-of-Roundness

During the EDM process, the tool tip is deformed. The images taken by a DINO camera at a magnification of 30.6× (Figure 17) show the same. There are two main reasons for the change in shape of the tool. The first one is the wear of tool tip, and the second is the rounding of the edge of the tool tip. The deformation in the shape of tool tip depends upon the process parameters. The effect of I_p on change in tool OOR during the EDM process is presented in Figure 18. A similar trend is observed between the DOE model and the machine-learning model. Both models show an increase in I_p for an increase in OOR. The discharge column also decomposes the tool electrode along with the removal of material. Due to increase in I_p, more heat is produced, thus increasing the distortion of tool electrode [32]. The images shown in Figure 19, captured by a DINO camera at a magnification of 30.6×, show the same trends. At lower I_p, there was less damage to the surface of tool and its corners. However, as the I_p increased, more edge wear of the tool tip was observed, which, in turn, made the edges of tool tip round and changed the profile of tool tip.

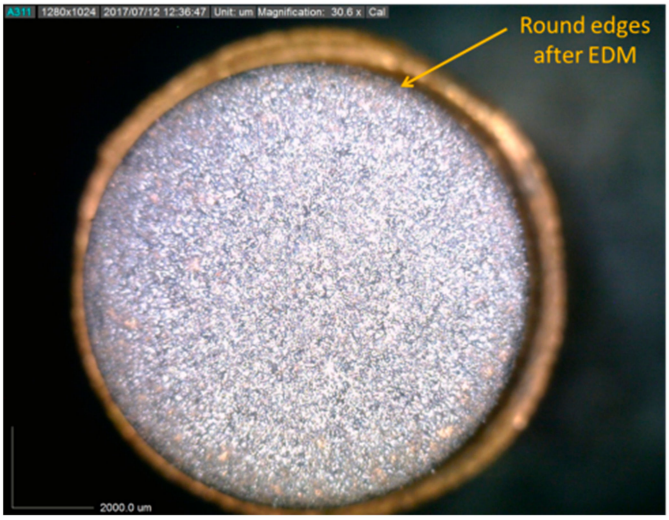

(**a**)

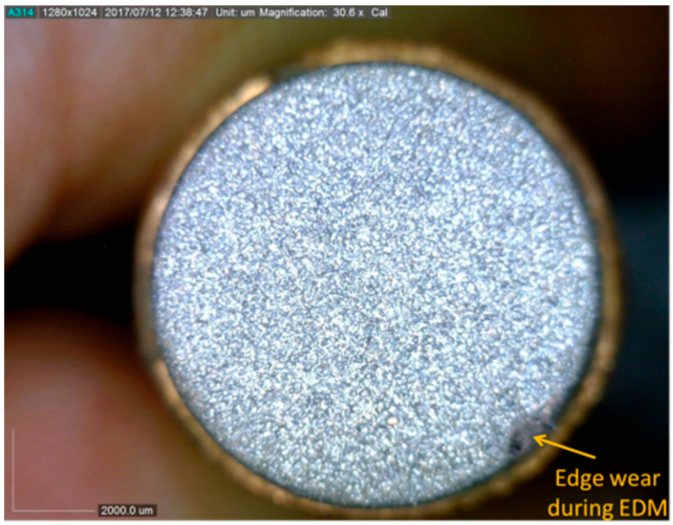

(**b**)

Figure 17. (**a**) Change in shape of tool tip after EDM. (**b**) Change in tool tip due to wear.

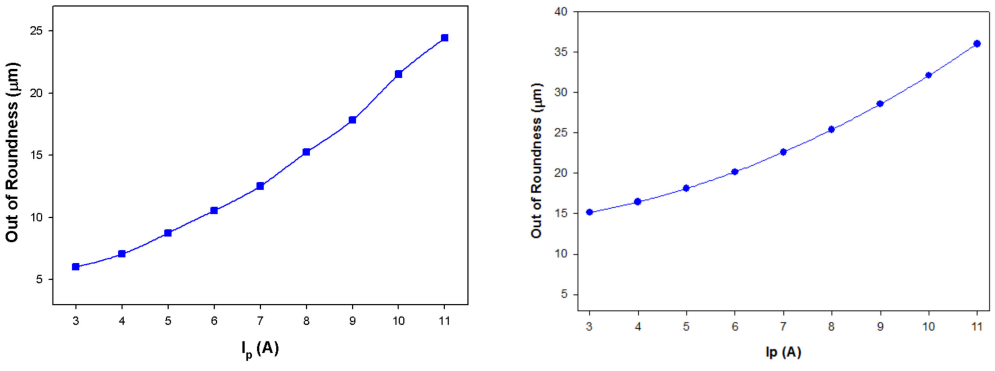

(**a**) (**b**)

Figure 18. Main effect plots for change in OOR with I_p using (**a**) DOE model; (**b**) machine learning model.

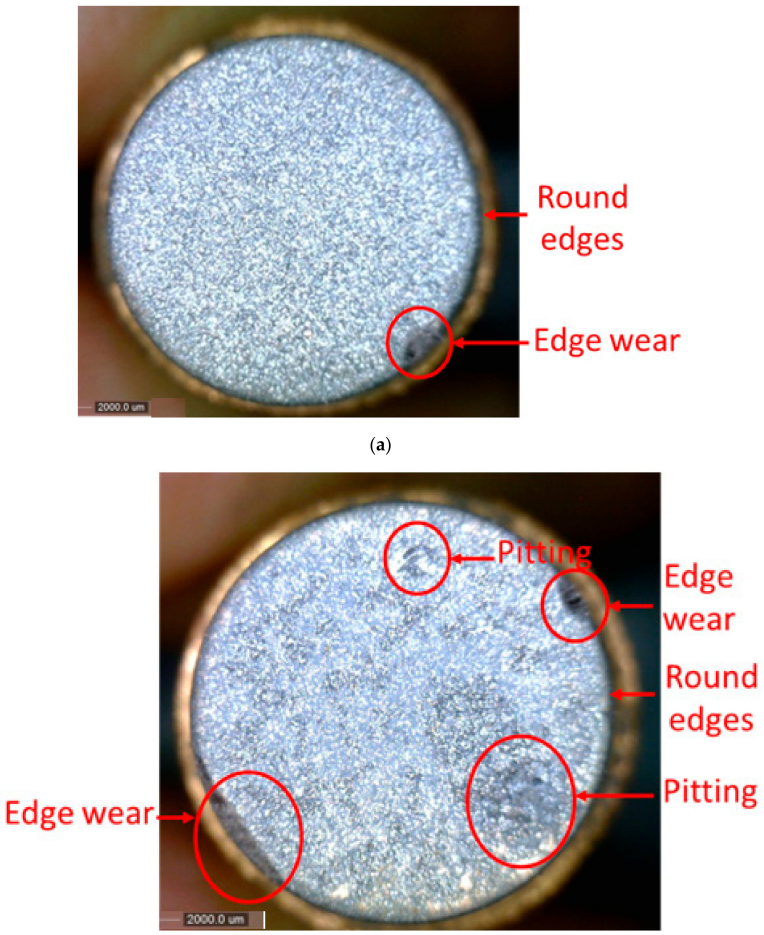

Figure 19. Variation in tool profile with I_p (I_p, V_g, T_{on}, T_{off}, P) (**a**) (7,60, 300, 30, 16); (**b**) (10, 60, 300, 30, 16); units as per Table 2.

The outcome of an increase in Ton on change in OOR for the EDM process is shown in Figure 20. It can be that change in OOR reduced as the Ton augmented. As the Ton amplified, diameter of the discharge column also enlarged, thereby reducing the energy density of the electrical discharge on the discharge spot [33].

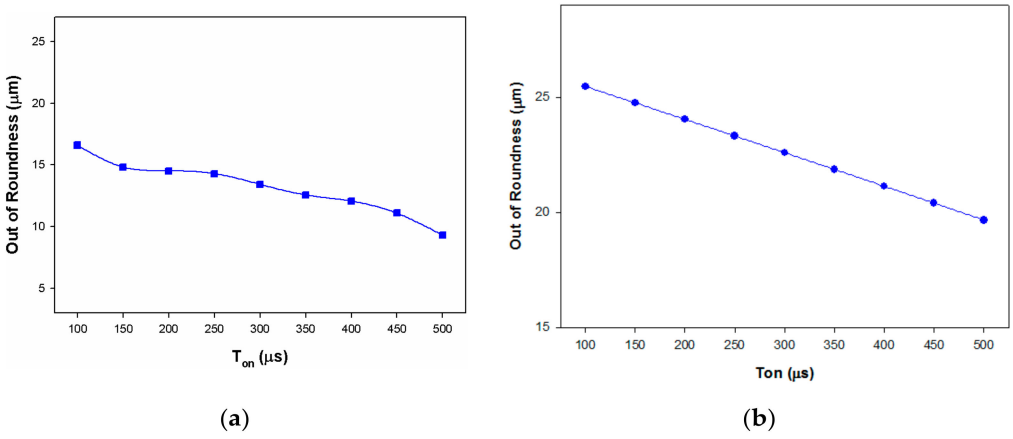

Figure 20. Main effect plots for change in OOR with T_{on} using (**a**) DOE model; (**b**) machine learning model.

In Figure 21, the images, captured by DINO camera at a magnification of 30.6×, show the effect of T_{on} on the surface and profile of the tool tip. The rounding of edges can be observed in Figure 21a,b, though at lower T_{on}, there is more damage to the surface of tool and its corners. The rounding of corners resulted in change in the roundness of tool tip, hence in the profile of tool.

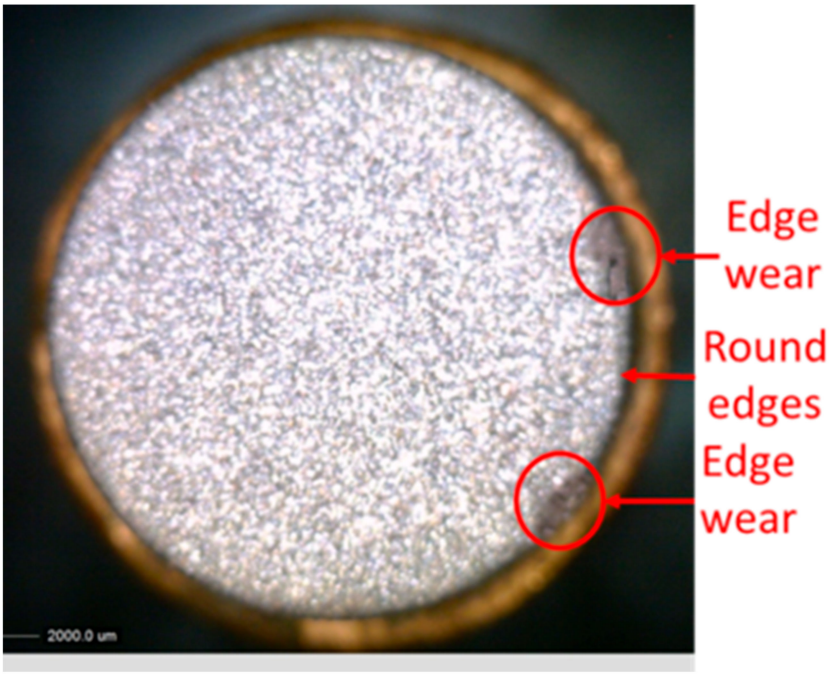

(**a**)

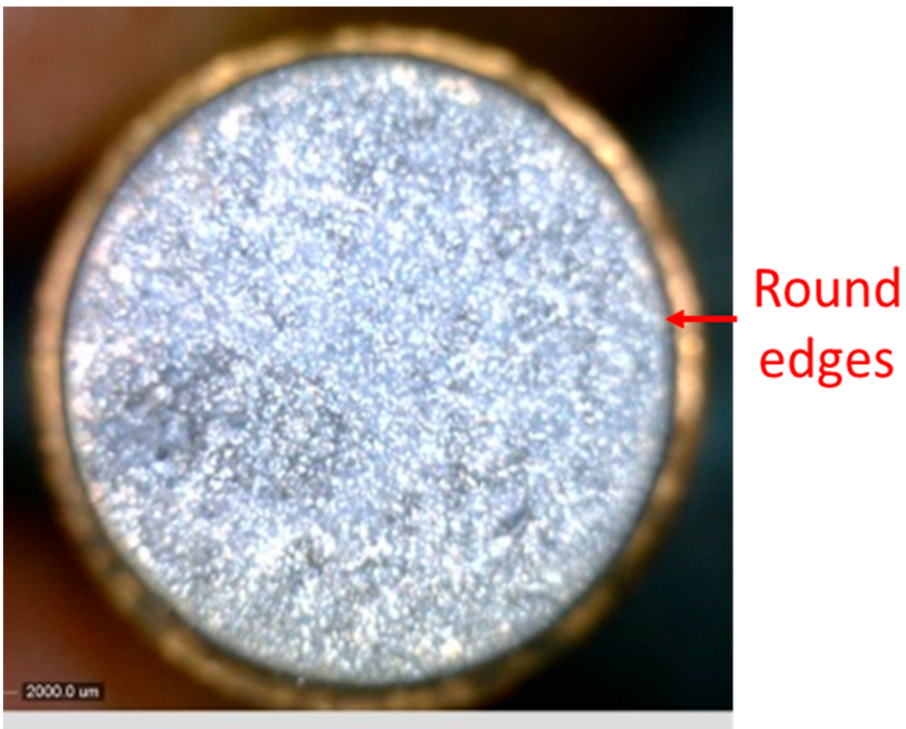

(**b**)

Figure 21. Variation in tool surface and profile with T_{on} (**a**) T_{on}= 300 µs (**b**) T_{on}= 450 µs; other process parameters I_p= 7 A, V_g= 60 V, T_{off}= 30 µs, P= 16 kgf/cm^2.

In the Figure 22, the impact of pulse off duration on change in OOR is shown. With an increase in the T_{off}, the change in OOR of the tool decreased. Due to smaller T_{off}, additional recurrent sparks are caused resulting in the generation of heat energy. This reheat will be ensnared in the tool due to lack of time for dissipation inducing extra deformation in the contour of the tool [34,35]. Figure 23 depicts these trends; in Figure 23a,b, captured by a DINO camera at a magnification of 30.6×, the rounding of edges can be observed, and not much difference in change in tool profile was recorded, though at lower, T_{off} there is slightly more damage to the surface of the tool and its corners.

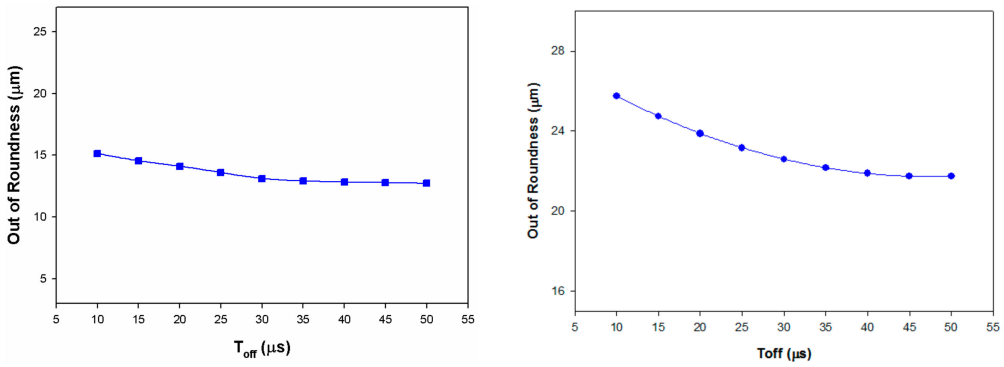

(**a**) (**b**)

Figure 22. Main effect plots for change in OOR with Toff using (**a**) DOE model; (**b**) machine learning model.

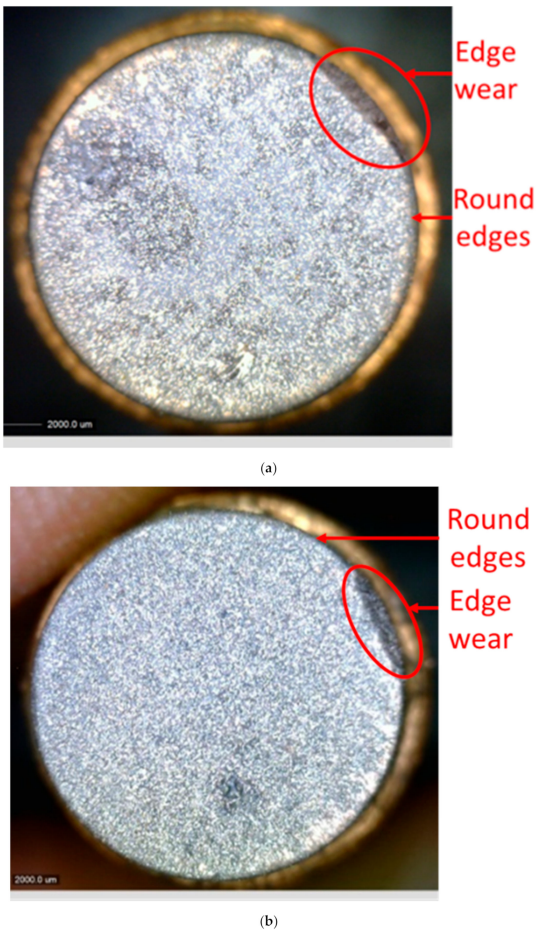

Figure 23. Variation in tool surface and profile with Toff (**a**) Toff = 30 µs (**b**) Toff = 45 µs; other process parameters Ip = 7 A, Vg = 60 V, Ton = 300 µs, P = 16 kgf/cm^2.

4. Confirmation Experiments

Confirmation experiments were carried out to check the accuracy of developed machine learning and DOE models for the prediction of SR and change in OOR. The machine learning-based regression equation succeeded in predicting SR with an error range of 0.40–2.85%, while the DOE-based regression equation predicted SR with an error range of 1.9–3.16% [28]. The average errors for machine learning and the DOE model were found to be 1.60% and 2.53%, respectively. Similarly, the machine learning-based regression equation succeeded in predicting change in ORR with an error range of 0.15–2.01%, while the DOE-based regression equation predicted it with an error range of 0.34–3.35%. The average errors for machine learning and the DOE model were found to be 0.48% and 1.53%, respectively. Figures 24 and 25 shows the comparison of the DOE model and the machine learning model for SR and change in OOR. It can be observed that the machine learning model for SR and change in OOR is more accurate as compared to the DOE-based model.

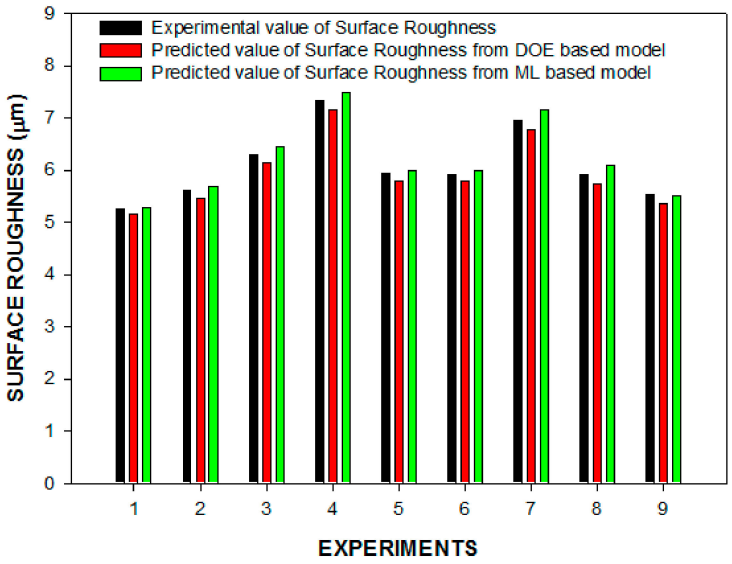

Figure 24. Comparison of DOE model and machine learning model with experimental findings for SR.

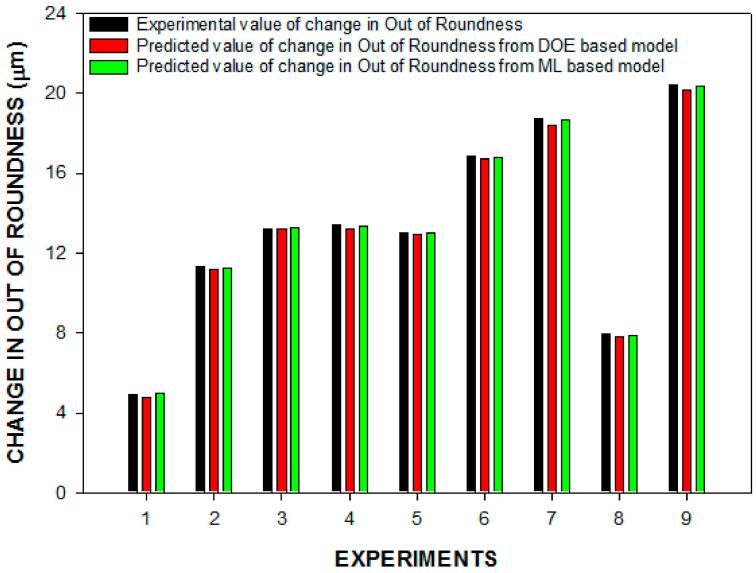

Figure 25. Comparison of DOE model and machine learning model with experimental findings for change in OOR.

Figure 26 shows the plot between the experimental and predicted value of SR and change in OOR. From the plot, it is clearly evident that there are no obvious pattern and unusual structure. The figure indicates the closeness among the observed data and the predicted results. This means that the developed models are adequate and can be used for analysis to determine effects of various parameters on SR and change in OOR.

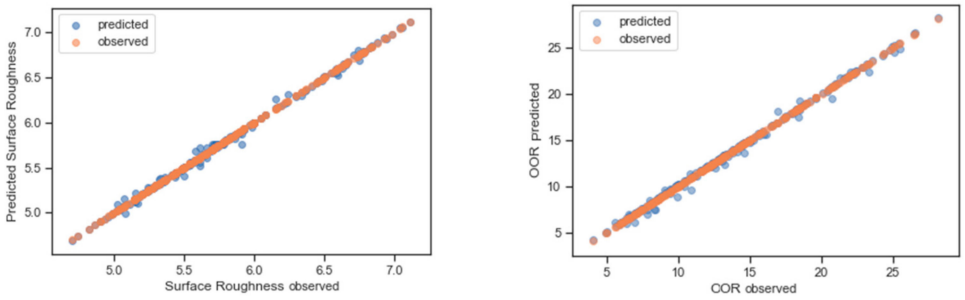

(**a**) (**b**)

Figure 26. Predicted versus observed for (**a**) surface roughness and (**b**) change in out-of-roundness.

5. Conclusions

- A machine learning-based model was trained for the prediction of SR and change in OOR by correlating the input parameters, namely I_p, V_g, T_{on}, T_{off} and P.
- With the help of heat maps and the probability table, it was found that Ip, Ton, Toff and P had significant effect on SR and that I_p, T_{on} and T_{off} affected OOR.
- An increase in SR was observed with an increase in I_p, T_{on} and T_{off}, whereas an inverse relation is observed between SR and P. The SEM micrographs of specimens machined at different input parameter settings also attested to these facts.
- The change in OOR increased with Ip and decreased with T_{on} and T_{off}. The images taken by the DINO camera at different settings of process parameters also corroborate the abovementioned findings.
- It was also observed that the trends obtained by using the DOE model and machine learning model for both the surface roughness and change in OOR exhibited similar tendencies.
- Machine learning-based regression equation predicted SR with an average error of 1.60% in comparison to 2.53% for DOE-based regression equation.
- During the prediction of change in OOR, the average errors for machine learning and DOE model were found to be 0.48% and 1.53%, respectively.
- The machine learning-based model is the best model to predict the surface roughness and change in OOR based on the selected process parameters and their ranges.

Author Contributions: Conceptualization, V.S. and K.V.; methodology, V.S. and K.V.; software, A.S.W. and K.V.; validation, A.S.W., V.S. and K.V.; formal analysis, V.S.; investigation, V.S. and K.V.; resources, A.S.W., V.S. and K.V.; writing—original draft preparation, A.S.W.; writing—review and editing, V.S. and K.V.; supervision, V.S. and K.V. All authors have read and agreed to the published version of the manuscript.

Funding: This research received no external funding.

Institutional Review Board Statement: Not applicable.

Informed Consent Statement: Not applicable.

Data Availability Statement: Relevant data are available from the corresponding author.

Conflicts of Interest: The authors declare no conflict of interest.

Appendix A

Table A1. Data set for machine learning-based regression model.

Sr. No.	I_p	V_g	T_{on}	T_{off}	P	SR (μm)	OOR (μm)	Sr. No.	I_p	V_g	T_{on}	T_{off}	P	SR (μm)	OOR (μm)
1	10	50	400	20	14	6.77	22.82	132	5	50	200	25	14	5.37	8.52
2	6	70	400	20	18	5.42	07.30	133	9	70	200	45	18	5.69	19.60
3	10	50	200	40	18	5.99	21.94	134	7	60	500	35	16	6.37	09.97
4	8	60	300	30	20	5.60	14.38	135	3	60	300	35	16	5.15	06.19
5	6	50	200	20	14	5.36	12.02	136	5	50	400	45	14	5.73	12.01
6	10	70	200	40	18	5.82	23.50	137	7	60	300	35	16	5.82	12.20
7	8	60	500	30	16	6.66	10.98	138	9	70	400	25	14	6.61	14.70
8	4	60	300	30	16	5.23	07.06	139	5	50	400	25	18	5.20	06.04
9	6	50	400	40	14	5.93	12.70	140	9	70	200	45	14	5.89	16.90
10	8	60	300	30	16	5.97	14.98	141	5	70	400	25	14	5.55	07.42
11	10	70	400	20	14	6.82	17.82	142	7	40	300	35	16	5.78	12.40
12	6	50	400	20	18	5.37	07.74	143	9	50	200	45	14	6.05	17.40
13	10	70	200	40	14	6.00	20.82	144	9	70	400	45	18	6.64	13.80
14	6	70	400	20	14	5.70	08.62	145	9	70	400	45	14	6.84	15.10
15	8	40	300	30	16	5.93	15.70	146	7	80	300	35	16	5.67	12.02
16	10	50	200	40	14	6.16	21.82	147	5	50	400	45	18	5.43	08.14
17	10	70	400	40	18	6.93	15.90	148	5	70	400	45	18	5.48	08.20
18	10	70	400	40	14	7.11	17.22	149	5	50	400	25	14	5.49	09.92
19	8	80	300	30	16	5.82	14.26	150	5	50	200	45	14	5.60	06.62
20	6	50	400	40	18	5.66	08.82	151	7	60	300	35	12	5.93	12.80
21	6	70	400	40	18	5.71	08.38	152	9	50	400	25	18	6.36	15.30
22	6	50	400	20	14	5.64	11.62	153	5	70	400	45	14	5.78	09.52
23	6	50	200	40	14	5.65	09.10	154	5	70	200	25	18	4.90	12.73
24	8	60	300	30	12	6.05	15.58	155	9	70	200	25	14	5.65	20.50
25	10	50	400	20	18	6.60	18.94	156	9	70	200	25	18	5.45	23.22
26	8	60	300	50	16	6.15	14.42	157	7	60	300	15	16	5.49	14.10
27	6	70	400	40	14	5.98	09.70	158	9	50	200	25	18	5.62	21.10
28	6	70	200	20	18	4.93	15.70	159	5	70	200	45	18	5.14	10.82
29	10	70	200	20	14	5.71	25.42	160	9	70	400	25	18	6.41	13.41
30	10	70	200	20	18	5.54	28.10	161	9	50	400	45	14	6.79	19.60
31	8	60	300	10	16	5.58	17.94	162	5	50	200	25	18	5.07	08.64
32	10	50	200	20	18	5.70	26.54	163	5	70	200	25	14	5.20	10.02
33	6	70	200	40	18	5.21	12.78	164	7	60	100	35	16	5.28	14.40
34	10	70	400	20	18	6.65	16.50	165	9	50	400	45	18	6.59	15.72
35	10	50	400	40	14	7.06	22.22	166	5	70	200	45	14	5.44	08.12
36	6	50	200	20	18	5.09	12.14	167	9	50	200	25	14	5.81	21.04
37	6	70	200	20	14	5.20	13.02	168	5	50	200	45	18	5.30	06.74
38	8	60	100	30	16	5.27	18.98	169	9	50	400	20	15	6.44	18.50

Table A1. *Cont.*

Sr. No.	I_p	V_g	T_{on}	T_{off}	P	SR (μm)	OOR (μm)	Sr. No.	I_p	V_g	T_{on}	T_{off}	P	SR (μm)	OOR (μm)
39	10	50	400	40	18	6.88	18.34	170	11	60	300	30	17	6.65	24.80
40	6	70	200	40	14	5.48	10.10	171	5	70	400	20	19	5.04	05.62
41	10	50	200	20	14	5.88	26.42	172	9	50	200	40	19	5.72	18.20
42	6	50	200	40	18	5.38	09.22	173	5	50	200	20	15	5.23	09.40
43	9	55	400	20	14	6.50	18.33	174	9	70	200	40	19	5.55	20.90
44	11	65	300	30	16	6.67	24.36	175	7	60	500	30	17	6.23	08.08
45	5	75	400	20	18	5.14	05.96	176	3	60	300	30	17	4.99	05.88
46	9	55	200	40	18	5.79	18.71	177	5	50	400	40	15	5.64	10.30
47	7	65	300	30	20	5.35	12.42	178	7	60	300	30	17	5.69	12.30
48	5	55	200	20	14	5.25	09.74	179	9	70	400	20	15	6.49	14.61
49	9	75	200	40	18	5.57	20.77	180	5	50	400	20	19	4.99	04.92
50	7	65	500	30	16	6.34	08.17	181	9	70	200	40	15	5.82	18.20
51	3	65	300	30	16	5.07	6.47	182	5	70	400	20	15	5.41	06.94
52	5	55	400	40	14	5.72	10.65	183	7	40	300	30	17	5.65	11.90
53	7	65	300	30	16	5.74	12.38	184	9	50	200	40	15	5.99	18.10
54	9	75	400	20	14	6.50	13.83	185	9	70	400	40	19	6.51	13.10
55	5	55	400	20	18	5.14	05.91	186	9	70	400	40	15	6.78	14.43
56	9	75	200	40	14	5.77	17.45	187	7	80	300	30	17	5.54	12.70
57	5	75	400	20	14	5.44	06.65	188	5	50	400	40	19	5.27	06.42
58	7	45	300	30	16	5.75	12.60	189	5	70	400	40	19	5.32	07.12
59	9	55	200	40	14	5.99	17.95	190	5	50	400	20	15	5.36	08.84
60	9	75	400	40	18	6.59	12.97	191	5	50	200	40	15	5.51	06.94
61	9	75	400	40	14	6.78	13.65	192	7	60	300	30	13	5.87	12.90
62	5	55	400	40	18	5.42	07.41	193	9	50	400	20	19	6.17	14.60
63	5	75	400	40	18	5.43	07.47	194	7	60	300	50	17	5.87	12.11
64	5	55	400	20	14	5.43	09.15	195	5	70	400	40	15	5.69	08.44
65	5	55	200	40	14	5.54	07.25	196	5	70	200	20	19	4.70	14.22
66	7	65	300	30	12	5.85	12.34	197	9	70	200	20	15	5.54	22.40
67	9	55	400	20	18	6.30	15.09	198	9	70	200	20	19	5.27	25.15
68	7	65	300	50	16	5.93	12.24	199	7	60	300	10	17	5.30	14.82
69	5	75	400	40	14	5.72	08.15	200	9	50	200	20	19	5.43	22.40
70	5	75	200	20	18	4.74	14.57	201	5	70	200	40	19	4.98	11.72
71	9	75	200	20	14	5.49	21.63	202	9	70	400	20	19	6.22	13.34
72	9	75	200	20	18	5.29	24.95	203	9	50	400	40	15	6.73	18.30
73	7	65	300	10	16	5.36	14.92	204	5	50	200	20	19	4.86	09.52
74	9	55	200	20	18	5.50	22.89	205	5	70	200	20	15	5.06	11.50
75	5	75	200	40	18	5.03	12.07	206	7	60	100	30	17	5.15	16.52
76	9	75	400	20	18	6.30	13.15	207	9	50	400	40	19	6.46	14.40
77	9	55	400	40	14	6.78	18.15	208	5	70	200	40	15	5.35	09.04
78	5	55	200	20	18	4.96	10.51	209	9	50	200	20	15	5.70	22.30

Table A1. *Cont.*

Sr. No.	I_p	V_g	T_{on}	T_{off}	P	SR (μm)	OOR (μm)	Sr. No.	I_p	V_g	T_{on}	T_{off}	P	SR (μm)	OOR (μm)
79	5	75	200	20	14	5.04	11.25	210	5	50	200	40	19	5.14	07.02
80	7	65	100	30	16	5.14	16.58	211	9	50	400	20	14	6.48	20.70
81	9	55	400	40	18	6.58	14.91	212	11	60	300	30	16	6.75	25.50
82	5	75	200	40	14	5.33	08.75	213	5	70	400	20	18	5.07	06.95
83	9	55	200	20	14	5.70	22.13	214	9	50	200	40	18	5.86	18.53
84	5	55	200	40	18	5.24	08.01	215	7	60	300	30	20	5.32	12.60
85	9	50	450	20	14	6.65	18.75	216	5	50	200	20	14	5.24	10.92
86	11	60	350	30	16	6.98	23.31	217	9	70	200	40	18	5.63	20.41
87	5	70	450	20	18	5.24	04.05	218	7	60	500	30	16	6.34	09.45
88	9	50	250	40	18	6.00	17.49	219	3	60	300	30	16	5.02	05.60
89	7	60	350	30	20	5.50	10.03	220	5	50	400	40	14	5.58	10.83
90	5	50	250	20	14	5.31	09.47	221	7	60	300	30	16	5.78	11.80
91	9	70	250	40	18	5.89	18.55	222	9	70	400	20	14	6.60	15.22
92	3	60	350	30	16	5.07	06.03	223	7	60	300	30	16	5.72	13.25
93	5	50	450	40	14	5.72	12.37	224	5	50	400	20	18	5.17	06.40
94	7	60	350	30	16	5.89	11.63	225	9	70	200	40	14	5.83	18.42
95	9	70	450	20	14	6.76	13.25	226	5	70	400	20	14	5.48	08.35
96	5	50	450	20	18	5.14	04.99	227	7	60	300	30	16	5.91	12.24
97	9	70	250	40	14	6.08	16.87	228	7	60	300	30	16	5.74	11.80
98	5	70	450	20	14	5.54	06.37	229	7	40	300	30	16	5.66	13.12
99	7	40	350	30	16	5.80	12.85	230	9	50	200	40	14	6.00	16.90
100	9	50	250	40	14	6.19	18.37	231	9	70	400	40	18	6.63	13.87
101	9	70	450	40	18	6.84	11.75	232	9	70	400	40	14	6.74	15.00
102	9	70	450	40	14	7.04	14.07	233	7	80	300	30	16	5.66	13.26
103	7	80	350	30	16	5.80	10.41	234	5	50	400	40	18	5.43	08.41
104	5	50	450	40	18	5.42	07.49	235	5	70	400	40	18	5.44	07.85
105	5	70	450	40	18	5.53	06.55	236	7	60	300	30	16	5.77	12.42
106	5	50	450	20	14	5.44	09.87	237	5	50	400	20	14	5.50	10.40
107	5	50	250	40	14	5.59	07.97	238	5	50	200	40	14	5.61	07.84
108	7	60	350	30	12	6.00	13.23	239	7	60	300	30	12	5.91	13.56
109	9	50	450	20	18	6.45	13.87	240	7	60	300	30	16	5.73	11.90
110	7	60	350	50	16	6.08	12.49	241	9	50	400	20	18	6.15	16.17
111	5	70	450	40	14	5.83	08.87	242	7	60	300	30	16	5.75	13.12
112	5	70	250	20	18	4.90	11.65	243	7	60	300	50	16	5.98	12.35
113	9	70	250	20	14	5.80	20.05	244	5	70	400	40	14	5.71	09.92
114	9	70	250	20	18	5.60	21.73	245	5	70	200	20	18	4.82	14.61
115	7	60	350	10	16	5.51	13.17	246	9	70	200	20	14	5.57	21.30
116	9	50	250	20	18	5.71	20.67	247	7	60	300	30	16	5.77	12.84
117	5	70	250	40	18	5.18	10.15	248	9	70	200	20	18	5.35	25.12
118	9	70	450	20	18	6.56	10.93	249	7	60	300	10	16	5.33	14.95
119	9	50	450	40	14	6.94	19.57	250	9	50	200	20	18	5.61	23.30

Table A1. *Cont.*

Sr. No.	I_p	V_g	T_{on}	T_{off}	P	SR (µm)	OOR (µm)	Sr. No.	I_p	V_g	T_{on}	T_{off}	P	SR (µm)	OOR (µm)
120	5	50	250	20	18	5.01	08.59	251	5	70	200	40	18	5.11	11.12
121	5	70	250	20	14	5.20	09.97	252	9	70	400	20	18	6.24	14.12
122	7	60	150	30	16	5.35	14.83	253	9	50	400	40	14	6.71	18.56
123	9	50	450	40	18	6.74	14.69	254	5	50	200	20	18	5.08	09.00
124	5	70	250	40	14	5.48	08.47	255	5	70	200	20	14	5.15	11.35
125	9	50	250	20	14	5.91	21.55	256	7	60	100	30	16	5.15	16.02
126	5	50	250	40	18	5.30	07.09	257	7	60	300	30	16	5.70	12.83
127	9	50	400	25	14	6.55	19.18	258	7	60	300	30	16	5.72	13.26
128	11	60	300	35	16	6.76	24.23	259	9	50	400	40	18	6.59	15.62
129	5	70	400	25	18	5.25	06.10	260	5	70	200	40	14	5.36	08.01
130	9	50	200	45	18	5.85	17.52	261	9	50	200	20	14	5.61	22.05
131	7	60	300	35	20	5.43	11.57	262	5	50	200	40	18	5.25	06.50

References

1. Ho, K.; Newman, S. State of the art electrical discharge machining. *Int. J. Mach. Tools Manuf.* **2003**, *43*, 1287–1300. [CrossRef]
2. Ahmed, A.; Tanjilul, M.; Fardin, A.; Wong, Y.; Rahman, M.; Kumar, A.S. On the design and application of hybrid electrical discharge and arc machining process for enhancing drilling performance in inconel 718. *Int. J. Adv. Manuf. Technol.* **2018**, *99*, 1825–1837. [CrossRef]
3. Fu, J.; Qiu, M.; Shen, L.; Kong, L.; Ma, J. On processing of Inconel718 through multi-channel discharge ablation. *J. Manuf. Process* **2020**, *57*, 462–468. [CrossRef]
4. Walia, A.S.; Srivastava, V.; Jain, V.; Bansal, S.A. Effect of TiC Reinforcement in the Copper Tool on Roundness during EDM Process. In *Advances in Materials Science and Engineering*; Springer: Singapore, 2020; pp. 125–135.
5. Fenggou, C.; Dayong, Y. The study of high efficiency and intelligent optimization system in edm sinking process. *J. Mater. Process. Technol.* **2004**, *149*, 83–87. [CrossRef]
6. Rangajanardhaa, G.; Rao, S. Development of hybrid model and optimization of surface roughness in electric discharge machining using artificial neural networks and genetic algorithm. *J. Mater. Process. Technol.* **2009**, *209*, 1512–1520.
7. Chattopadhyay, K.D.; Verma, S.; Satsangi, P.S.; Sharma, P.C. Development of empirical model for different process parameters during rotary electrical discharge machining of copper–steel (EN-8) system. *J. Mater. Process. Technol.* **2009**, *209*, 1454–1465. [CrossRef]
8. Torres, A.; Puertas, I.; Luis, C.J. Modelling of surface finish, electrode wear and material removal rate in electrical discharge machining of hard-to-machine alloys. *Precis. Eng.* **2015**, *40*, 33–45. [CrossRef]
9. Raja, S.B.; Pramod, C.V.S.; Krishna, K.V.; Raghunathan, A.; Vinesh, S. Optimization of electrical discharge machining parameters on hardened die steel using Firefly Algorithm. *Eng. Comput* **2015**, *31*, 1–9. [CrossRef]
10. Choudhuri, B.; Sen, R.; Ghosh, S.K.; Saha, S.C. Modelling and multi-response optimization of wire electric discharge machining parameters using response surface methodology and grey–fuzzy algorithm. *Proc. Inst. Mech. Eng. B J. Eng. Manuf.* **2017**, *231*, 1760–1774. [CrossRef]
11. Payal, H.; Maheshwari, S.; Bharti, P.S. Process modeling of electric discharge machining of Inconel 825 using artificial neural network. *Int. J. Mech. Mechatron. Eng.* **2017**, *11*, 562–566.
12. Nain, S.S.; Sihag, P.; Luthra, S. Performance evaluation of fuzzy-logic and BP-ANN methods for WEDM of aeronautics super alloy. *MethodsX* **2018**, *5*, 890–908. [CrossRef]
13. Thankachan, T.; Prakash, K.S.; Malini, R.; Ramu, S.; Sundararaj, P.; Rajandran, S.; Rammasamy, D.; Jothi, S. Prediction of surface roughness and material removal rate in wire electrical discharge machining on aluminum based alloys/composites using Taguchi coupled Grey Relational Analysis and Artificial Neural Networks. *Appl. Surf. Sci.* **2019**, *472*, 22–35. [CrossRef]
14. Sahu, S.K.; Naik, S.; Das, S.R.; Dhupal, D. Parametric Optimization of Surface Roughness and Overcut in Electric Discharge Machining of Al-SiC Using Copper Electrode. In *Renewable Energy and its Innovative Technologies*; Springer: Singapore, 2019; pp. 99–116.
15. Rajneesh, R.; Subhash, S.; Mulik, R.S.; Kaushik, P. Study of Machining Performance in EDM through Response Surface Methodology. In *Advances in Industrial and Production Engineering*; Springer: Singapore, 2019; pp. 207–219.
16. Singh, N.K.; Singh, Y. Experimental Investigation and Modeling of Surface Finish in Argon-Assisted Electrical Discharge Machining Using Dimensional Analysis. *Arab. J. Sci. Eng.* **2019**, *44*, 5839–5850. [CrossRef]

17. Ulas, M.; Aydur, O.; Gurgenc, T.; Ozel, C. Surface roughness prediction of machined aluminum alloy with wire electrical discharge machining by different machine learning algorithms. *J. Mater. Res. Technol.* **2020**, *9*, 12512–12524. [CrossRef]
18. Bharti, P.S. Two-step optimization of electric discharge machining using neural network based approach and TOPSIS. *J. Interdiscip. Math.* **2020**, *23*, 81–96. [CrossRef]
19. Srivastava, V.; Pandey, P.M. Study of ultrasonic assisted cryogenically cooled EDM process using sintered (Cu–TiC) tooltip. *J. Manuf. Process* **2013**, *15*, 158–166. [CrossRef]
20. Walia, A.S.; Jain, V.; Srivastava, V. Development and performance evaluation of sintered tool tip while EDMing of hardened steel. *Mater. Res. Express* **2019**, *6*, 086520. [CrossRef]
21. Srivastava, V.; Pandey, P.M. Study of the cryogenically cooled electrode shape in electric discharge machining process. *World Acad. Sci. Eng. Technol.* **2011**, *60*, 1017–1021.
22. Srivastava, V.; Pandey, P.M. Performance evaluation of electrical discharge machining (EDM) process using cryogenically cooled electrode. *Mater. Manuf. Process* **2012**, *27*, 683–688. [CrossRef]
23. Walia, A.S.; Srivastava, V.; Jain, V. Fabrication and Application of Composite Electrodes in Electrical Discharge Machining-A Review. *Int. J. Comput. Appl.* **2018**, *4*, 1–5.
24. Li, L.; Wong, Y.S.; Fuh, J.Y.H.; Lu, L. EDM performance of TiC/Copper-based sintered electrodes. *Mater. Des.* **2001**, *22*, 669–678. [CrossRef]
25. Li, L.; Wong, Y.S.; Fuh, J.Y.H.; Lu, L. Effect of TiC in copper tungsten electrodes on EDM performance. *J. Mater. Process. Technol.* **2001**, *113*, 563–567. [CrossRef]
26. Srivastava, V. Experimental Investigations and Analysis of Electrical Discharge Machining Using Ultrasonic Assisted Cryogenically Cooled Electrode. Ph.D. Thesis, Indian Institute of Technology Delhi, New Delhi, India, 2013.
27. Das, M.K.; Kumar, K.; Barman, T.K.; Sahoo, P. Application of artificial bee colony algorithm for optimization of MRR and surface roughness in EDM of EN31 tool steel. *Procedia Mater. Sci.* **2014**, *6*, 741–751. [CrossRef]
28. Kiran, M.B.; Ramamoorthy, B.; Radhakrishnan, V. Evaluation of surface roughness by vision system. *Int. J. Mach. Tools Manuf.* **1998**, *38*, 685–690. [CrossRef]
29. Mamalis, A.G.; Vosniakos, G.C.; Vaxevanidis, N.M.; Prohaszka, J. Macroscopic and microscopic phenomena of electro-discharge machined surfaces: An experimental investigation. *J. Mech. Work. Technol.* **2017**, *15*, 335–356. [CrossRef]
30. Xiuming, L.; Zhaoyao, S. Development and application of convex hull in the assessment of roundness error. *Int. J. Mach. Tools Manuf.* **2008**, *48*, 135–139. [CrossRef]
31. Walia, A.S. Experimental Investigations and Analysis of Electrical Discharge Machining of Hardened EN31 Steel Using Cermet Tool Tip. Ph.D. Thesis, Thapar Institute of Engineering & Technology, Patiala, India, 2020.
32. Khan, M.A.R.; Rahman, M.M.; Kadirgama, K. An experimental investigation on surface finish in die-sinking EDM of Ti-5Al-2.5Sn. *Int. J. Adv. Manuf. Technol.* **2015**, *77*, 1727–1740. [CrossRef]
33. Walia, A.S.; Srivastava, V.; Jain, V. Impact of copper-titanium carbide tooltip on machined surface integrity during electrical discharge machining of EN31 steel. *Mater. Res. Express* **2019**, *6*, 106582. [CrossRef]
34. Pandey, P.C.; Jilani, S.T. Plasma channel growth and the resolidified layer in EDM. *Precis. Eng.* **1986**, *8*, 104–110. [CrossRef]
35. Dijck, F.S.V.; Dutre, W.L. Heat conduction model for the calculation of the volume of molten metal in electric discharges. *J. Phys. D Appl. Phys.* **1974**, *7*, 899–910. [CrossRef]